

Dielectronic recombination data for dynamic finite-density plasmas

XV. The silicon isoelectronic sequence

Jagjit Kaur¹, T. W. Gorczyca¹, and N. R. Badnell²

¹Department of Physics, Western Michigan University, Kalamazoo, MI 49008, USA

²Department of Physics, University of Strathclyde, Glasgow G4 0NG, UK
e-mail: gorczyca@wmich.edu

ABSTRACT

Context. We aim to present a comprehensive theoretical investigation of dielectronic recombination (DR) of the silicon-like isoelectronic sequence and provide DR and radiative recombination (RR) data that can be used within a generalized collisional-radiative modelling framework.

Aims. Total and final-state level-resolved DR and RR rate coefficients for the ground and metastable initial levels of 16 ions between P⁺ and Zn¹⁶⁺ are determined.

Methods. We carried out multi-configurational Breit-Pauli (MCBP) DR calculations for silicon-like ions in the independent processes, isolated resonance, distorted wave (IPIRDW) approximation. Both $\Delta n_c = 0$ and $\Delta n_c = 1$ core excitations are included using *LS* and intermediate coupling schemes.

Results. Results are presented for a selected number of ions and compared to all other existing theoretical and experimental data. The total dielectronic and radiative recombination rate coefficients for the ground state are presented in tabulated form for easy implementation into spectral modelling codes. These data can also be accessed from the Atomic Data and Analysis Structure (ADAS) OPEN-ADAS database. This work is a part of an assembly of a dielectronic recombination database for the modelling of dynamic finite-density plasmas.

Key words. Atomic data – Atomic processes – plasmas

1. Introduction

The emission of electromagnetic radiation from cosmic plasmas, as a consequence of electron-ion collision processes, reveals information about physical parameters of the plasma such as chemical composition, pressure, electronic or ionic temperature, and density. However, the accuracy of these parameters is strongly influenced by uncertainties in the ionization balance calculations, which are in turn affected by uncertainties in the ionization and recombination rate coefficients. Therefore, it is of fundamental interest to determine accurate rate coefficients for astrophysical and laboratory plasma studies.

Dielectronic recombination (DR) — Burgess (1964, 1965) — is the dominant electron-ion recombination process in most photoionized and (electron) collisionally ionized plasmas. In collisionally ionized plasmas (e.g. stars and supernovae remnants), the ionization occurs due to electrons and ions that are formed at a temperature approximately half of their ionization potential (Bryans et al. 2006). On the other hand, in photoionized plasmas (e.g. H II regions and planetary nebulae), ionization occurs due to photons and ions that are formed at temperatures below the ionization energies (Ferland et al. 1998; Kallman & Bautista 2001). Therefore, the ionization balance is achieved over very different temperature ranges in collisionally ionized and photoionized plasmas. To model the spectral emission, plasma modelling codes, including CLOUDY (Ferland et al. 1998) and XSTAR (Kallman & Bautista 2001), for photoionized plasmas, and the CHIANTI code (Landi et al. 2006), for collisionally ionized plasmas, require accurate DR rate coef-

ficients over a wide range of temperatures to determine the elemental abundances and, therefore, plasma parameters.

In order to address the need for accurate DR rate coefficients, a large collaborative effort was initiated by Badnell et al. (2003) to calculate the total and final-state level-resolved DR rate coefficients from the ground and the metastable states of all ionization stages of all ions up to Zn relevant to the modelling of astrophysical and laboratory plasmas. In a series of papers, multiconfiguration Breit-Pauli (MCBP) calculations have been performed to provide a DR database for all isoelectronic sequences of the first and second row ions and third row ions up through Al-like (Abdel-Naby et al. 2012; Altun et al. 2004, 2006, 2007; Badnell 2006a; Bautista & Badnell 2007; Colgan et al. 2004, 2003; Mitnik & Badnell 2004; Zatsarinny et al. 2006, 2004a, 2003, 2004b) and also Ar-like (Nikolić et al. 2010). Final-state level-resolved DR rate coefficients are necessary for modelling plasmas within the collisional-radiative framework at densities found in astrophysical plasmas, such as solar flares ($> 10^{12} \text{ cm}^{-3}$) (Polito et al. 2016a,b), and in magnetic fusion plasmas for example ITER ($10^{12} - 10^{15} \text{ cm}^{-3}$) (Watts et al. 2013), where the coronal approximation is not valid. DR data for initial metastable states are required for modelling plasmas with timescales comparable to the life time of the metastable states. The first unaddressed isoelectronic sequence in the third row is silicon-like, for which no systematic calculations have been performed. Here, we present a reliable DR database for the Si-like isoelectronic sequence.

Bryans et al. (2009a) have demonstrated the effect of inaccuracies in DR data for singly-charged ions in the low-temperature regime of molecular clouds, causing significant differences in

the abundances of species found on the surface of dust grains and in the gas-phase. They have used RR rate coefficients of singly-charged ions from the UMIST database (Woodall et al. 2007) in chemical models; however, the origin of this RR data is unclear. There are no other RR data, while DR data exist for P^+ , S^+ , Cl^+ , and Fe^+ . Our present study of the silicon-like iso-electronic sequence finally provides state-of-the-art calculations of the RR and DR rate coefficients for P^+ , for instance, that are needed to constrain the chemical models used to study the evolution of dense molecular clouds, protostars, and diffuse molecular clouds. Such studies are in turn important for understanding the origin of the first organic molecules.

Furthermore, the difference in the sulphur abundances in planetary nebulae derived from an ionization correction factor (ICFs), and the spectral emission line measurements from the expected value observed by Henry et al. (2012), constitute the motivation to update the S^{2+} DR data, as was done for totals by Badnell et al. (2015). Henry et al. (2012) demonstrated how uncertainties in the positions of low-lying resonances affect the low-temperature DR rate coefficients, that in turn affect the elemental abundances in planetary nebulae. The present study extends the previous theoretical work by determining partial as well the total rate coefficients, and including the $\Delta n_c = 1$ core excitation, in addition to $\Delta n_c = 0$ core excitation.

Additionally, accurate DR rate coefficients for M-shell Fe^{12+} are needed to accurately model the absorption features needed to reproduce the so-called unresolved transition array (UTA). This is a series of inner-shell absorption lines at 15 – 17 Å, caused by $2p \rightarrow 3d$ photoabsorption in the X-ray spectrum of Active Galactic Nuclei (AGN), as observed by Chandra and XMM-Newton. The problem has been attributed in part to the underestimated low-temperature DR rate coefficients for M-shell Fe used in the photoionization models (Badnell 2006b). The recent benchmark theoretical and experimental total DR results are presented by Hahn et al. (2014) for M-shell Fe^{12+} ions.

The remainder of this paper is organized as follows: In Sect. 2 we discuss the theoretical methodology and outline the present calculations. We then present the results for total dielectronic and radiative recombination rate coefficients and compare with earlier theoretical and experimental results in Sect. 3. Finally, we summarize the assembly of final data in Sect. 4.

2. Theory

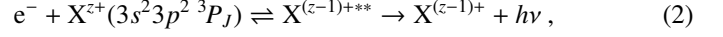
A detailed description of our theoretical calculations has already been given by Badnell et al. (2003). Here we outline only the main points. The atomic structure and collision code AUTOSTRUCTURE (Badnell 2011) was used to perform DR calculations. A multi-configuration Breit-Pauli (MCBP) method is implemented within an independent processes, isolated resonance, distorted-wave (IPIRDW) approximation, whereby radiative and dielectronic recombination processes are treated independently, neglecting interference between the two, which is valid for plasma applications (Pindzola et al. 1992). The code is based on lowest-order perturbation theory, for which both the electron-photon and electron-electron interactions are treated to first order. Energy levels, radiative rates, and autoionization rates were calculated in LS and intermediate coupling (IC) approximations. We note that the spin-independent mass-velocity and Darwin relativistic operators are included in LS coupling, as well as in IC coupling. The wave functions for the N -electron

target system are written as a configuration expansion,

$$\Psi_i = \sum_{j=1}^N c_{ij} \phi_j, \quad (1)$$

where c_{ij} are the mixing coefficients that are chosen so as to diagonalize $\langle \Psi_i | H | \Psi_j \rangle$, where H is the Breit-Pauli Hamiltonian. The set of basis functions are constructed from Slater determinants using the one-electron spin-orbitals.

The dielectronic recombination process for silicon-like ions can be represented schematically as



where z represents the degree of ionization for the ion X . The basis set consisting of the $3s^2 3p^2$, $3s^2 3p 3d$, $3s 3p^3$, $3s 3p^2 3d$, $3s^2 3d^2$, $3s 3p 3d^2$, $3p^4$ and $3p^3 3d$ configurations (assuming a closed shell Ne-like core) was used to define the silicon-like target states, for the (by far dominant) $\Delta n_c = 0$ core excitation. The one-electron spin-orbitals were obtained using the Thomas-Fermi-Dirac-Amaldi (TFDA) model potential (Eissner & Nussbaumer 1969), and were optimized by varying the scaling parameters λ_{nl} so as to reproduce the fine-structure splitting of the $3s^2 3p^2 \ ^3P_J$ levels, to within 0.0005 Ryd compared to NIST. Table 1 lists the optimized scaling parameters for the entire iso-electronic sequence.

The $(N + 1)$ -electron basis was constructed by coupling a valence orbital, nl , or a continuum orbital, ϵl , to the N -electron target configurations, and also included the $3s^2 3p^3$, $3s^2 3p^2 3d$, $3s^2 3p 3d^2$, $3s 3p^4$, $3s 3p^3 3d$, $3s 3p^2 3d^2$, $3s^2 3d^3$, $3s 3p 3d^3$, $3p^5$, $3p^4 3d$ and $3p^3 3d^2$ configurations. Distorted wave calculations were performed to generate the bound nl ($n > 3$) and continuum orbitals. The wave functions constructed using this $(N + 1)$ -electron basis were used to determine the autoionization and radiative rates, which are then assembled to obtain the final-state level-resolved and total dielectronic recombination rate coefficients for all silicon-like ions.

For the valence electron, n -values were included up to 25, and a quantum defect approximation for high n up to 1000 was used (Badnell et al. 2003). The values for the orbital quantum numbers were included up to $l = 8$. For intershell ($\Delta n_c = 1$) core excitation from the $n = 3$ shell, the N -electron target basis set was comprised of $3s^2 3p^2$, $3s^2 3p 3d$, $3s 3p^3$, and $3s 3p^2 3d$ configurations in addition to configurations arising from $3\ell \rightarrow 4\ell'$ excitations (for $\ell = 0-1$ & $\ell' = 0-3$). The $(N + 1)$ -electron target basis was described by coupling a valence orbital $4\ell'$ to the N -electron configurations for ($\Delta n_c = 1$) core excitation plus either coupling a valence orbital nl , or a continuum orbital ϵl , to the N -electron target configurations. Values of the principal quantum number included were $n \leq 25$, and of the continuum/valence electron orbital angular momentum were $\ell' \leq 5$. A quantum defect approximation is included for $25 < n \leq 1000$.

The partial dielectronic recombination rate coefficient α_{if} from an initial state i to a final, recombined state f is given in the IPIRDW approximation as (Burgess 1964)

$$\alpha_{if}(T) = \left(\frac{4\pi a_0^2 I_H}{k_B T} \right)^{3/2} \sum_d \frac{\omega_d}{2\omega_i} \exp\left(-\frac{E_c}{k_B T_e}\right) \times \frac{\sum_{\ell} A_{d \rightarrow i, E_{ct}}^a A_{d \rightarrow f}^r}{\sum_h A_{d \rightarrow h}^r + \sum_{m, \ell} A_{d \rightarrow m, E_{ct}}^a}, \quad (3)$$

where the outer sum is over all accessible $(N + 1)$ -electron doubly excited resonance states d , of statistical weight ω_d , ω_i is the

statistical weight of the N -electron target state, A^a and A^r are the autoionization and radiative rates (the sums over h and m gives rise to the total widths), and E_c is the energy of the continuum electron, which is fixed by the position of the resonances. Here, I_H is the ionization potential energy of the hydrogen atom, k_B is the Boltzmann constant, and T is the electron temperature. The total dielectronic recombination rate coefficient is obtained by summing over all the recombined final states f ,

$$\alpha_i^{(tot)}(T) = \sum_f \alpha_{if}(T). \quad (4)$$

Partial and total RR rate coefficients were also computed using the same N - and $(N + 1)$ -electron configurations as for the $\Delta n_c = 0$ core excitation DR calculations, but with no doubly-excited (resonance) states $X^{(z-1)+**}$.

3. Results

The final-state level-resolved partial dielectronic recombination rate coefficients, from both ground and metastable initial levels, were computed and then tabulated in the ADAS (Summers 2003) *adf09* format. The total ($\Delta n_c = 0$ plus $\Delta n_c = 1$) intermediate coupling DR rate coefficients were also fitted according to the formula

$$\alpha_i^{DR}(T) = \frac{1}{T^{3/2}} \sum_i c_i \exp\left(-\frac{E_i}{T}\right), \quad (i \leq 8). \quad (5)$$

The fitting coefficients c_i and E_i for DR rate coefficients from the ground state are listed in Table 2 for the entire silicon-like isoelectronic sequence. Our fits reproduce the actual computed data to better than 5% for all ions over the temperature range $z^2(10^1 - 10^7)$ K, where z is the residual charge of the recombining ion. In fact, the accuracy is better than 1% over the collisionally-ionized plasma region.

Also, the total RR rate coefficients were computed, tabulated in ADAS format, and fitted using the formula of Verner & Ferland (1996),

$$\alpha_i^{RR}(T) = A \sqrt{T_0/T} \left[\left(1 + \sqrt{T/T_0}\right)^{1-B} \left(1 + \sqrt{T/T_1}\right)^{1+B} \right]^{-1}, \quad (6)$$

where, for low-charge ions, we replace B by (Gu 2003),

$$B \rightarrow B + C \exp(-T_2/T). \quad (7)$$

Partial RR rate coefficients are tabulated according to the ADAS (Summers 2003) *adf48* format. The RR fitting coefficients are also listed in Table 3. These fits are accurate to better than 5% over the temperature range $z^2(10^1 - 10^7)$ K.

We compare our present IC total Maxwellian-averaged DR rate coefficients of a selected number of ions along the silicon-like isoelectronic sequence to other available theoretical and experimental results. In particular, we compare to the widely used recommended data of Mewe et al. (1980) and Mazzotta et al. (1998). Mewe et al. (1980) developed a single fitting formula, based on the data of Ansari et al. (1970) and Jacobs et al. (1977), for all ions and for all temperatures. The previously recommended database of Mazzotta et al. (1998) was derived from the calculations of Jacobs et al. (1977, 1979, 1980), which were then fitted by Shull & Van Steenberg (1982), for even numbered nuclei, and interpolated to provide the data for odd numbered nuclei by Landini & Monsignori Fossi (1991). Also, indicated in the figures are the temperature regions of collisionally-ionized

and photoionized plasmas. These temperature ranges are determined for each ion by considering the range of temperatures for which the ion's fractional abundance is 90% or more of its maximum value. The collisionally-ionized zones were obtained using the calculations of Bryans et al. (2009b), and the photoionized zones have been computed using CLOUDY (Ferland et al. 1998). We note that the DR data used in those Si-like abundance calculations were those of Mazzotta et al. (1998), not including our present DR rate coefficients.

In Fig. 1, we show the total DR rate coefficients for the ground state of S^{2+} . A comprehensive treatment of S^{2+} DR for $3 \rightarrow 3$ ($\Delta n_c = 0$) core excitation has recently been performed by Badnell et al. (2015). The present calculations are performed using the same MCBP IPIRDW approach as in the previous work, but we also include the small contributions from the $3 \rightarrow 4$ ($\Delta n_c = 1$) core excitations, unlike in the previous work. As detailed more fully in the earlier work by Badnell et al. (2015), the DR resonance contributions to the rate coefficient can be classified into one of three categories. First, there are contributions from the well-known dipole resonances (Burgess 1964) — those that accumulate to a dipole-allowed, core-excited S^{2+} thresholds, such as the $3s^2 3p 3d(^3D)nl$ Rydberg series. These give rise to the characteristic high-temperature DR rate coefficient peak at temperatures $\frac{3}{2}kT \sim$ ionization limit.

As seen in Fig. 1, both MCBP calculations are in good agreement at high temperatures.

The second category of resonance contributions is due to the fine-structure induced, core-excited states, such as the $3s^2 3p^2(^3P_{1,2})nl$ Rydberg series. These resonances only contribute at low energies — below the fine-structure splitting of the Si-like $3s^2 3p^2\ ^3P$ ground term — and therefore the corresponding Rydberg series consist of high- n resonances ($22 \leq n \leq 32$ for all sequences). This latter series yields a DR rate coefficient that peaks (and dominates) at low temperatures $\frac{3}{2}kT \sim$ fine-structure splitting.

The third category of resonances encountered are the so-called “ $(N + 1)$ -electron resonances” — low-lying $n = 3$ dipole resonances such as $3s 3p^3 3d$, in the case of this sequence. These DR resonance contributions are the most uncertain due to the corresponding uncertainty in energy position, as discussed in the earlier case of S^{2+} (Badnell et al. 2015). To obtain total DR rate coefficients at 10^4 K consistent with that required to determine the sulphur abundance in the Orion Nebula, a photoionized plasma, Badnell et al. (2015) shifted the positions of these $n = 3$ resonances to lower energies. This adjustment was further justified by simpler MCHF structure comparisons for the near-threshold, bound $(N + 1)$ -electron states of S^+ , indicating that the computed $(N + 1)$ -electron energy positions were indeed higher than the experimental values for bound states (Badnell et al. 2015). For consistency, we make the same shift for S^{2+} of $\Delta E_{N+1} = -0.157$ Ryd.

Also in Fig. 1, the present results are compared with other available data including the LS coupling results of Badnell (1991), using AUTOSTRUCTURE, and the LS coupling R -matrix results of Nahar (1995), which include both RR and DR contributions. We note that the recommended data set of Mazzotta et al. (1998) for S^{2+} appears to use the high-temperature R -matrix results of Nahar (1995).

At this point, it is worth discussing the expected accuracy of our computed DR results, especially as it pertains to the three different categories of resonances. The first dipole core series, as treated in the original Burgess (1964) formulation, peaks at a high temperature given by the Rydberg series limit $n \rightarrow \infty$ energy positions and core oscillator strengths, the latter being com-

puted fairly accurately in general. Provided that we perform the empirical shift of each core Rydberg limit to the experimental values (Ralchenko et al. 2011), thereby shifting every Rydberg member by the same energy, we expect to minimize the uncertainty in the high-temperature dipole-dominated DR rate coefficient.

In the same manner, the fine-structure resonances, that contribute strongly at lower temperatures, are governed by $n \rightarrow \infty$ Rydberg series, with limits given by the fine-structure splitting of the S^{2+} ground state. In fact, the minimum n of each Rydberg series is given by $-Z^2/n^2 \approx$ fine-structure splitting, giving $n \geq 22$ for all series, and minimizing the resonance energy uncertainty. Provided that the calculations reproduce, or empirically shift to, the fine-structure split Si-like experimental energies (Ralchenko et al. 2011), we minimize the uncertainty in these resonance contributions.

The third type of $(N + 1)$ -electron resonance contributions carry the largest uncertainty, as discussed more fully in Badnell et al. (2015) for the case of S^{2+} . This uncertainty in rate coefficient contribution is due to the corresponding, relatively large, uncertainty in the resonance energy positions of the low-lying ($n = 3$) Rydberg members. However, as we discuss further below, the $(N + 1)$ -electron states all eventually become bound for higher ionization states: only for lower charge states are some of the $(N + 1)$ -electron states autoionizing, thereby contributing to DR. Furthermore, the total uncertainties become negligible at even lower charge-states, as we will now demonstrate by looking at the next highest charge states: Cl^{3+} and Ar^{4+} .

In Fig. 2, we show total DR rate coefficients for the ground state of Cl^{3+} , separating the $n = 3$ $(N + 1)$ -electron contribution (about 50% of the total for $T = 2 \times 10^4 K$) from the total. In view of this strong contribution and the uncertainties known to be associated with resonance energy uncertainties here, it is important to try and establish the temperatures where the DR rate coefficients are affected, and by how much. Unfortunately, NIST does not give any autoionizing energies for Cl^{2+} . Furthermore, they give no bound energies for either of the two lowest lying configurations which give rise to autoionizing states ($3s^2 3p^3 3d^2$ and $3s 3p^3 3d$). Consequently, we can only use observed energies from $3s^2 3p^2 3d$ to guide us to a plausible shift of the resonances. Even here the doublets and quartets show different levels of agreement and it is only practical to use a single global shift which applies to all resonances. We choose it to be the largest difference, ~ 0.12 Ryd, which is already smaller than the $\sim 0.2 - 0.4$ Ryd case of S^+ (Badnell et al. 2015). Thus, we empirically lower the $(N + 1)$ -electron resonances by -0.12 Ryd and this gives rise to an increase the total DR rate coefficient of $\sim 10\%$ at photoionized plasma temperatures (see Fig. 2). Our present results are also compared to the earlier results of Mazzotta et al. (1998) and Mewe et al. (1980), both of which are based on LS calculations that lack any low-temperature fine-structure DR contributions that are included in our calculations. For comparison, the total RR rate coefficient for Cl^{3+} is also shown.

In Fig. 3, we show total DR rate coefficients for the ground state of Ar^{4+} , again showing just the contribution from the $n = 3$ resonances as well. For this higher-ionized system, the $3s 3p^3 3d(^4D_{7/2})$ state that dominated the low- T S^{2+} DR rate coefficient, due to its large oscillator strength and near-threshold positioning, is now bound. However, other $n = 3$ resonances still contribute to the low-temperature DR — the ionization stage is still relatively low — but their contribution to the total is only about 15% at $T = 3 \times 10^4$ K. Furthermore, the rate coefficient is found to be fairly insensitive to the uncertainty in $n = 3$ reso-

nance positions. Lowering them by -0.12 Ryd only results in an increase of a few percent at photoionized plasma temperatures (too small to be shown separately).

We also compare our results to the previously published final-state level-resolved rate coefficients of Arnold et al. (2015). Although both present and previous calculations used the same methodology, there are some important differences. First, a different basis set of N -electron target configurations was used in the previous work. Second, the previous work also used a different scaling parameter for each orbital whereas the same scaling parameter was used for all the orbitals in the present work, as listed in Table 1. Third, the previous work also shifted the N -electron target energies relative to the NIST values. We see from Fig. 3 that the present DR rate coefficient is less than the previous value by about 50% in the photoionized plasma zone and by about 10% in the collisionally-ionized plasma zone. The low temperature difference is a little large, even allowing for its uncertainty in a low-charge ion. We checked that the use of further observed energies had negligible effect. Instead, it appears (Loch, private communication, 2017) that an incorrect input dataset was used by Arnold et al. (2015). The intended dataset gives results much more in line with ours.

As seen in Fig. 3, the recommended data of Mewe et al. (1980) and Mazzotta et al. (1998), based on LS high-temperature calculations, do not reproduce the fine-structure resolved IC DR, for two reasons. First, the fine-structure splitting gives rise to additional Rydberg series near threshold, thereby increasing the low-temperature DR rate coefficient. Second, as discussed in Abdel-Naby et al. (2012), at higher temperatures and for states of sufficiently high n , fine-structure autoionization within terms of doubly-excited states, and subsequent fine-structure autoionization following radiative decay, is responsible for additional DR suppression, giving high-temperature IC results that are lower than the LS ones.

Continuing along the series for higher ionization stages, we note that our findings for K^{5+} are similar to those for Ar^{4+} — about 15% contribution from the $(N + 1)$ -electron resonances — while for Ca^{6+} these resonances contribute at most 5% to the total DR rate coefficient. Higher-charged ions have negligible contribution. Conversely, the $(N + 1)$ -electron resonance contributions for P^+ are small as well, about 5%, because the strongest of these resonances are high enough in energy (and remain so under any reasonable shift) that they are dominated by, and masked by, the stronger dipole resonances. Thus, likely only for S^{2+} (Badnell et al. 2015) do we have a significant uncertainty in the total DR rate coefficients at photoionized plasma temperatures due to the uncertainty in energy positions of the $(N + 1)$ -electron resonances.

In Fig. 4, we compare our intermediate-coupling DR rate coefficients, for Fe^{12+} forming Fe^{11+} via $3 \rightarrow 3$ ($\Delta n_c = 0$) and $3 \rightarrow 4$ ($\Delta n_c = 1$) core excitations, to experimental measurements, carried out using the heavy-ion Test Storage Ring (TSR) at the Max-Planck Institute for Nuclear Physics in Heidelberg (Hahn et al. 2014). We also compare our present DR data to previous MCBP (AUTOSTRUCTURE) calculations by Hahn et al. (2014), finding a difference of less than 10% in the photoionized plasma region and by about 5% in the collisionally-ionized plasma region. Similar to Hahn et al. (2014), the present theoretical rate coefficient is smaller than the experimental value, by approximately 30% in the photoionized region and 25% in the collisionally ionized region. This somewhat largish discrepancy cannot be explained by any inaccuracies discussed earlier for the three different types of resonances (indeed, all $(N + 1)$ -electron states are strongly bound by Fe^{12+}). Instead, a fourth type of res-

onance contribution error was discussed by Hahn et al. (2014). At higher ionization stages, the core-excited N -electron states, such as $3s^2 3pn_c l_c$ ($3 < n_c < \infty$) contribute more to the total DR, and our computational termination at $n_c = 4$ means that $5 \leq n_c$ contributions are neglected. These could account for much of the discrepancy: assuming a pure n_c^{-3} scaling beyond $n_c = 4$, the contributions from $n_c \geq 5$ increase the total DR rate coefficient by 15–25% over $10^6 - 10^9$ K. But, it should be noted that increasing Auger suppression with increasing n_c can be expected to reduce this amount somewhat. On the other hand, it cannot be ruled out that the experiment is in fact too high by about 25%, which is roughly the total calibration uncertainty in the experiments. Finally, we note also that the previous results of Mazzotta et al. (1998); Mewe et al. (1980), that are based on LS -coupling calculations, do not take into account fine-structure-induced DR and therefore do not show any low-temperature enhancement, as seen in Fig. 4.

In Fig. 5, we show the total DR rate coefficients from metastable as well as ground initial states of Fe^{12+} . We note first that the DR rate coefficients are LS -term dependent. Second, at low temperature there is a significant difference among DR from the three fine-structure split levels $3s^2 3p^2$ (3P_0), $3s^2 3p^2$ (3P_1) and $3s^2 3p^2$ (3P_2). The $3s^2 3p^2$ (3P_0) level-resolved DR is enhanced by second and third fine-structure-split Rydberg series near threshold whereas the $3s^2 3p^2$ (3P_1) DR has only the second fine-structure-split Rydberg series near threshold, and the $3s^2 3p^2$ (3P_2) series has no fine-structure-split Rydberg series enhancement near threshold. Also shown in Fig. 5 are the present RR results from both the ground and metastable initial levels of Fe^{12+} .

We present in Fig. 6 the DR rate coefficients for both $\Delta n_c = 0$ ($3 \rightarrow 3$) and $\Delta n_c = 1$ ($3 \rightarrow 4$) core excitations, for selected ions along the silicon-like sequence. Also shown are the total ($\Delta n_c = 0 + \Delta n_c = 1$) DR rate coefficients. For low-charged Ar^{4+} , the contribution from $3 \rightarrow 4$ core excitation to the total DR rate coefficient is negligible. Additionally, using a configuration-averaged distorted wave method, Arnold et al. (2015) also showed that the contribution from $\Delta n_c = 2$ core excitation to the total rate coefficient is 3 to 4 orders of magnitude smaller than the sum of the contributions from $\Delta n_c = 0$ and $\Delta n_c = 1$ core excitations. The $3 \rightarrow 4$ core excitation contributions are less than 1% for Ti^{8+} , and 2% for V^{9+} , whereas, for Zn^{16+} , the $\Delta n_c = 1$ contribution leads to an increase of approximately 15% in the total DR rate coefficient.

Lastly, in Fig. 7, we compare our present Maxwellian-averaged DR rate coefficients (in IC), for the entire silicon-like isoelectronic sequence, to the recommended data of Mazzotta et al. (1998). The recommended data is based-upon calculations that do not take explicit account of fine-structure and therefore do not show DR contributions at low temperatures that arise from fine-structure Rydberg series near threshold. This deficiency becomes greater with increase in the effective charge z . At higher temperatures, the two sets of results differ appreciably, especially for low- z ions. For example, there is a difference of about 50% for P^+ and 30% for Cl^{3+} .

Also, note that the final results and the fitting coefficients listed in Table 2 correspond to the unshifted calculations.

4. Summary

We have carried-out multi-configuration intermediate-coupling Breit-Pauli calculations for total and partial (final-state level-resolved) DR and RR rate coefficients for all ions from P^+ through Zn^{16+} of the silicon-like isoelectronic sequence. We

have compared total dielectronic recombination rate coefficients with other theoretical and experimental results. Good agreement is found at higher temperatures. At lower temperatures that are applicable to photoionized plasmas, our new results include additional DR contributions that were not included in most previous results, and differ markedly from the recommended results of Mazzotta et al. (1998). We have also investigated the contributions from the low-lying ($N + 1$)-electron resonances to the low-temperature total DR rate coefficient. The uncertainties associated with these contributions are likely significant only for S^{2+} (Badnell et al. 2015). Fitting coefficients for total DR and RR rate coefficients from the ground state were presented. Partial DR and RR rate coefficients are archived in OPEN-ADAS¹ using the ADAS *adf09* and *adf48* formats, respectively. These data are needed for both astrophysical and fusion plasma modelling and constitute part of a dielectronic recombination database assembly for modelling dynamic finite-density plasmas in general (Badnell et al. 2003).

References

- Abdel-Naby, S. A., Nikolić, D., Gorczyca, T. W., Korista, K. T., & Badnell, N. R. 2012, *A&A*, 537, A40
- Altun, Z., Yumak, A., Badnell, N. R., Colgan, J., & Pindzola, M. S. 2004, *A&A*, 420, 775
- Altun, Z., Yumak, A., Badnell, N. R., Loch, S. D., & Pindzola, M. S. 2006, *A&A*, 447, 1165
- Altun, Z., Yumak, A., Yavuz, I., et al. 2007, *A&A*, 474, 1051
- Ansari, S. M. R., Elwert, G., & Mücklich, P. 1970, *Z. Naturforsch.*, 25a, 1781
- Arnold, I., Thomas, E., Loch, S. D., Abdel-Naby, S., & Ballance, C. P. 2015, *Journal of Physics B Atomic Molecular Physics*, 48, 175005
- Badnell, N. R. 1991, *ApJ*, 379, 356
- Badnell, N. R. 2006a, *A&A*, 447, 389
- Badnell, N. R. 2006b, *ApJ*, 651, L73
- Badnell, N. R. 2011, *Computer Physics Communications*, 182, 1528
- Badnell, N. R., Ferland, G. J., Gorczyca, T. W., Nikolić, D., & Wagle, G. A. 2015, *ApJ*, 804, 100
- Badnell, N. R., O’Mullane, M. G., Summers, H. P., et al. 2003, *A&A*, 406, 1151
- Bautista, M. A. & Badnell, N. R. 2007, *A&A*, 466, 755
- Bryans, P., Badnell, N. R., Gorczyca, T. W., et al. 2006, *ApJS*, 167, 343
- Bryans, P., Kreckel, H., Roueff, E., Wakelam, V., & Savin, D. W. 2009a, *ApJ*, 694, 286
- Bryans, P., Landi, E., & Savin, D. W. 2009b, *ApJ*, 691, 1540
- Burgess, A. 1964, *ApJ*, 139, 776
- Burgess, A. 1965, *ApJ*, 141, 1588
- Colgan, J., Pindzola, M. S., & Badnell, N. R. 2004, *A&A*, 417, 1183
- Colgan, J., Pindzola, M. S., Whiteford, A. D., & Badnell, N. R. 2003, *A&A*, 412, 597
- Eissner, W. & Nussbaumer, H. 1969, *Journal of Physics B Atomic Molecular Physics*, 2, 1028
- Ferland, G. J., Korista, K. T., Verner, D. A., et al. 1998, *PASP*, 110, 761
- Gu, M. F. 2003, *ApJ*, 590, 1131
- Hahn, M., Badnell, N. R., Grieser, M., et al. 2014, *ApJ*, 788, 46
- Henry, R. B. C., Speck, A., Karakas, A. I., Ferland, G. J., & Maguire, M. 2012, *ApJ*, 749, 61
- Jacobs, V. L., Davis, J., Kepple, P. C., & Blaha, M. 1977, *ApJ*, 211, 605
- Jacobs, V. L., Davis, J., Rogerson, J. E., & Blaha, M. 1979, *ApJ*, 230, 627
- Jacobs, V. L., Davis, J., Rogerson, J. E., et al. 1980, *ApJ*, 239, 1119
- Kallman, T. & Bautista, M. 2001, *ApJS*, 133, 221
- Landi, E., Del Zanna, G., Young, P. R., et al. 2006, *ApJS*, 162, 261
- Landini, M. & Monsignori Fossi, B. C. M. 1991, *A&AS*, 91, 183
- Mazzotta, P., Mazzitelli, G., Colafrancesco, S., & Vittorio, N. 1998, *A&AS*, 133, 403
- Mewe, R., Schrijver, J., & Sylwester, J. 1980, *A&AS*, 40, 323
- Mitnik, D. M. & Badnell, N. R. 2004, *A&A*, 425, 1153
- Nahar, S. N. 1995, *ApJS*, 101, 423
- Nikolić, D., Gorczyca, T. W., Korista, K. T., & Badnell, N. R. 2010, *A&A*, 516, A97
- Pindzola, M. S., Badnell, N. R., & Griffin, D. C. 1992, *Phys. Rev. A*, 46, 5725
- Polito, V., Del Zanna, G., Dudík, J., et al. 2016a, *A&A*, 594, A64
- Polito, V., Reep, J. W., Reeves, K. K., et al. 2016b, *ApJ*, 816, 89

¹ <http://open.adas.ac.uk>

- Ralchenko, Y., Kramida, A. E., Reader, J., & NIST ASD Team. 2011, National Institute of Standards and Technology, <http://physics.nist.gov/asd>
- Shull, J. M. & Van Steenberg, M. 1982, *ApJS*, 48, 95
- Summers, H. P. 2003, ADAS User Manual (v2.6), available from <http://www.adas.ac.uk/manual.php>
- Verner, D. A. & Ferland, G. J. 1996, *ApJS*, 103, 467
- Watts, C., Udintsev, V., Andrew, P., et al. 2013, *Nuclear Instruments and Methods in Physics Research A*, 720, 7
- Woodall, J., Agúndez, M., Markwick-Kemper, A. J., & Millar, T. J. 2007, *A&A*, 466, 1197
- Zatsarinny, O., Gorczyca, T. W., Fu, J., et al. 2006, *A&A*, 447, 379
- Zatsarinny, O., Gorczyca, T. W., Korista, K., Badnell, N. R., & Savin, D. W. 2004a, *A&A*, 426, 699
- Zatsarinny, O., Gorczyca, T. W., Korista, K. T., Badnell, N. R., & Savin, D. W. 2003, *A&A*, 412, 587
- Zatsarinny, O., Gorczyca, T. W., Korista, K. T., Badnell, N. R., & Savin, D. W. 2004b, *A&A*, 417, 1173

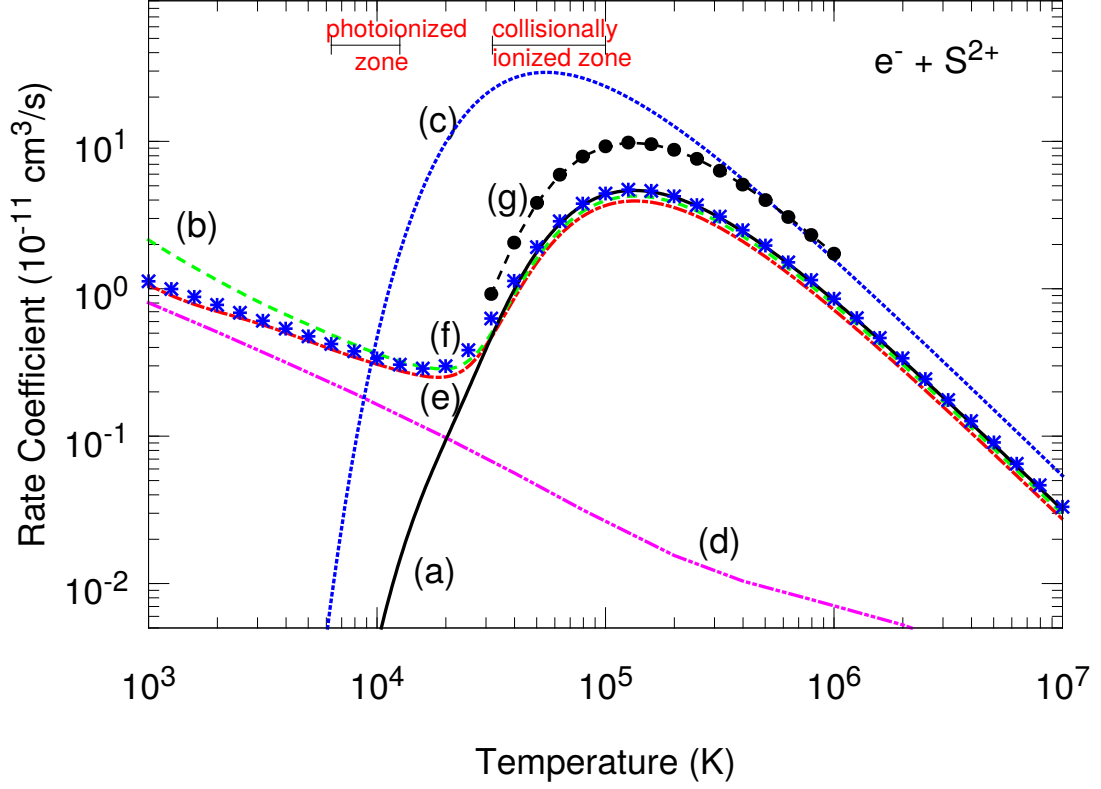


Fig. 1. Total Maxwellian-averaged DR and RR ground-state rate coefficients for S^{2+} : (a) *black solid curve*, previous recommended data of Mazzotta et al. (1998); (b) *green dashed curve*, present MCBP results; (c) *blue dotted curve*, empirical formula of Mewe et al. (1980); (d) *magenta dotted-dashed curve*, present RR rate coefficient; (e) *red dotted-dashed curve*, previous MCBP results (Badnell et al. 2015); (f) *blue asterisks*, *LS R-matrix*, RR + DR (Nahar 1995); (g) *black dashed curve with points*, *LS MCBP* results (Badnell 1991).

Table 1. Radial scaling parameters for orbitals ($1s$, $2s$, $2p$, $3s$, $3p$, $3d$, $4s$, $4p$, $4d$ and $4f$) used in the present study for $\Delta n_c = 0$ and $\Delta n_c = 1$ core-excitations in the silicon-like isoelectronic sequence.

Ion	P^+	S^{2+}	Cl^{3+}	Ar^{4+}	K^{5+}	Ca^{6+}	Sc^{7+}	Ti^{8+}	V^{9+}	$Cr^{10+} - Zn^{16+}$
λ_{nl}	1.114	1.13	1.12	1.125	1.15	1.15	1.16	1.17	1.18	1.185

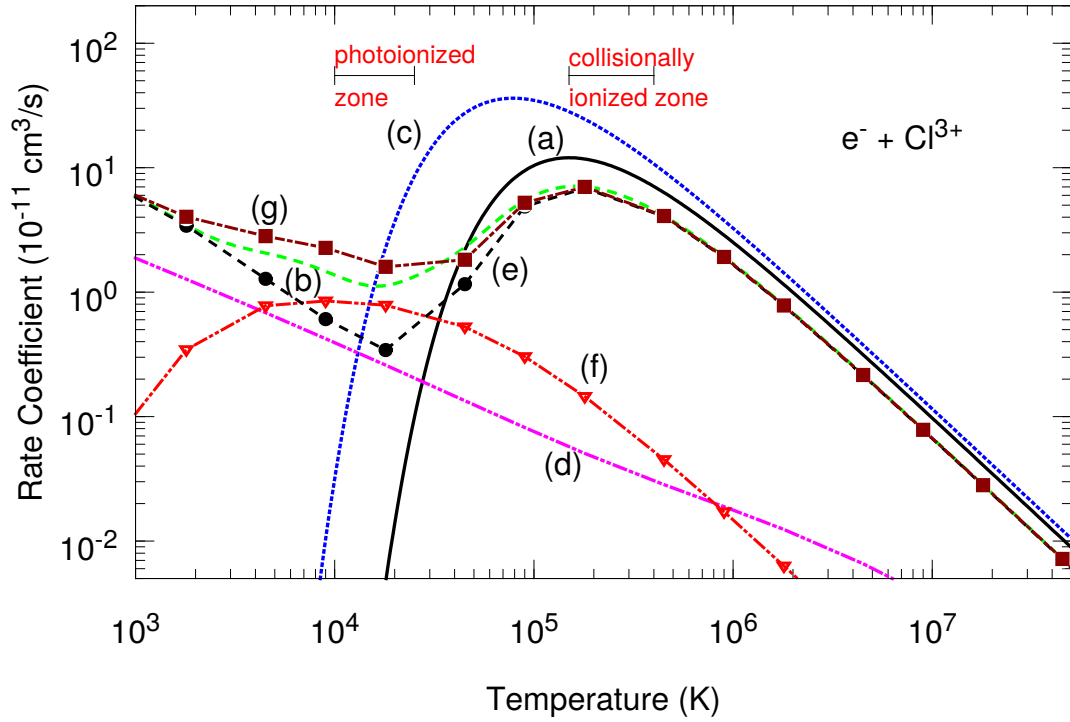


Fig. 2. Total Maxwellian-averaged DR and RR ground-state rate coefficients for Cl^{3+} : (a) *black solid curve*, previous recommended data of Mazzotta et al. (1998); (b) *green dashed curve*, present MCBP results; (c) *blue dotted curve*, empirical formula of Mewe et al. (1980); (d) *magenta dotted-dashed curve*, present RR rate coefficient; (e) *black dashed curve with filled circles*, present DR rate coefficients omitting $n = 3$ resonance contributions; (f) *red dotted-dashed curve with filled triangles*, present DR rate coefficients including only the $n = 3$ resonance contributions; (g) *brown dashed curve with filled squares*, present DR rate coefficients with the $n=3$ resonances lowered by -0.12 Ryd.

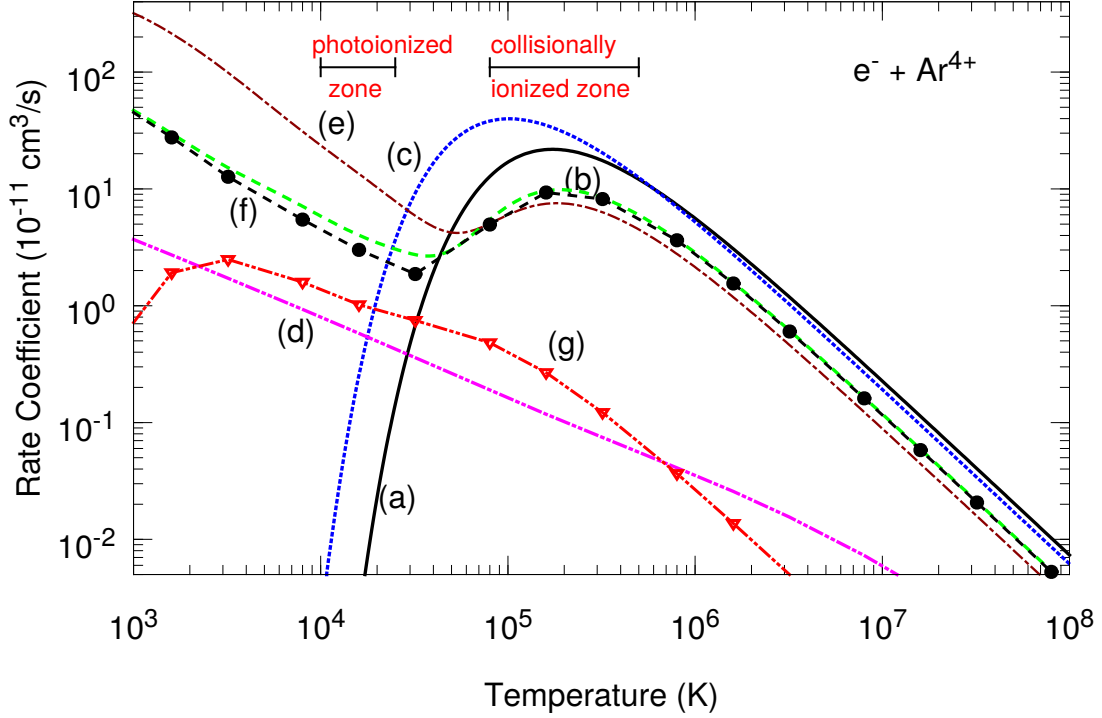


Fig. 3. Total Maxwellian-averaged DR and RR ground-state rate coefficients for Ar^{4+} : (a) *black solid curve*, previous recommended data of Mazzotta et al. (1998); (b) *green dashed curve*, present MCBP results; (c) *blue dotted curve*, empirical formula of Mewe et al. (1980); (d) *magenta dotted-dashed curve*, present RR rate coefficient; (e) *red dotted-dashed curve*, previous MCBP results of Arnold et al. (2015). (f) *black dashed curve with filled circles*, present DR rate coefficients omitting $n = 3$ resonance contributions; (g) *red dotted-dashed curve with filled triangles*, present DR rate coefficients including only the $n = 3$ resonance contributions.

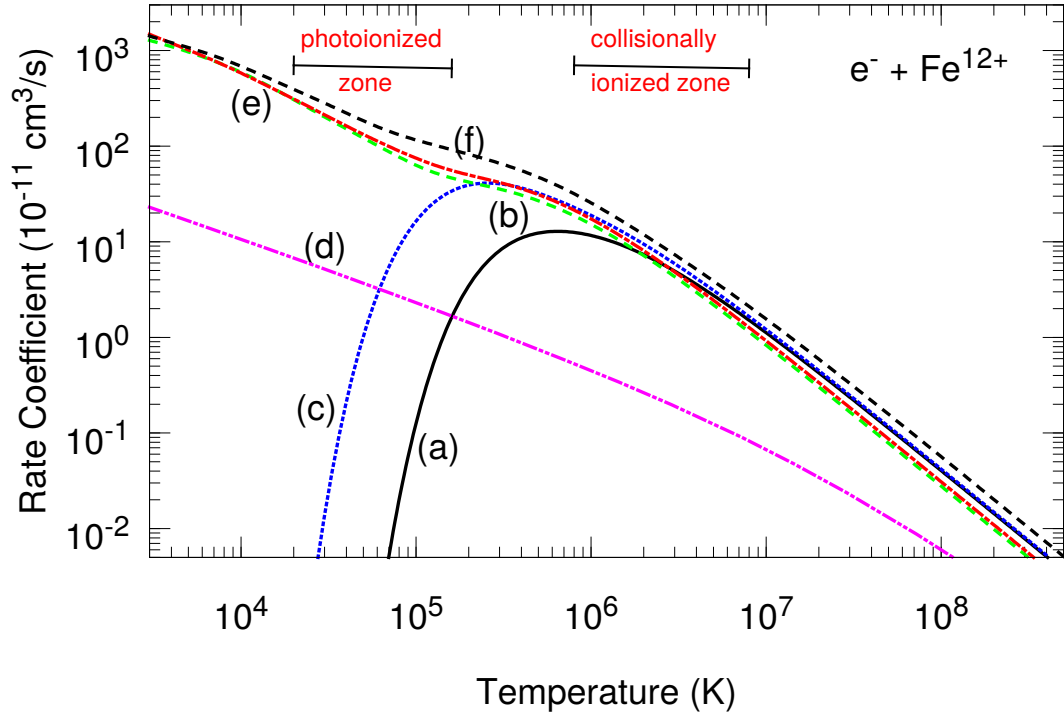


Fig. 4. Total Maxwellian-averaged DR and RR ground-state rate coefficients for Fe^{12+} : (a) *black solid curve*, previous recommended data of Mazzotta et al. (1998); (b) *green dashed curve*, present MCBP results; (c) *blue dotted curve*, empirical formula of Mewe et al. (1980); (d) *magenta dotted-dashed curve*, present RR rate coefficient; (e) *red dotted-dashed curve*, previous MCBP results presented in Hahn et al. (2014); and (f) *black dashed curve*, experimental measurements (Hahn et al. 2014).

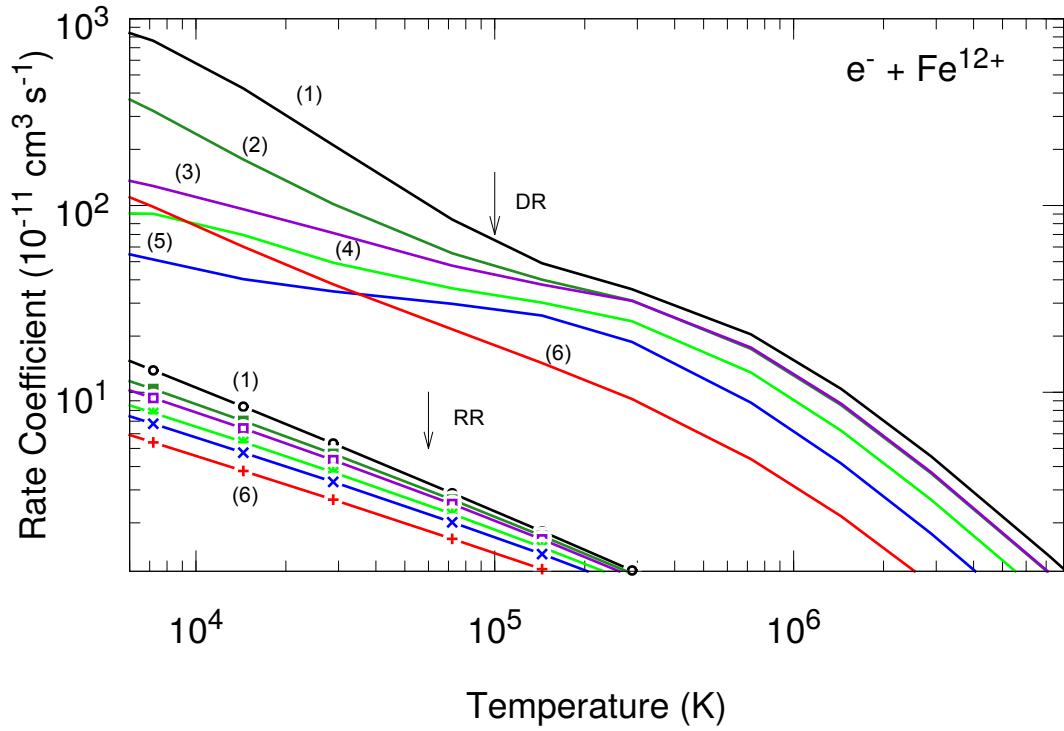


Fig. 5. Total Maxwellian-averaged DR and RR rate coefficients from the ground ($3s^23p^2$ (3P_0) ($i = 1$)) and metastable initial levels ($3s^23p^2$ ($^3P_{1,2}, ^1D_2, ^1S_0$) ($i = 2 - 5$) and $3s^23p3d$ (5S_2) ($i = 6$)) of Fe^{12+} .

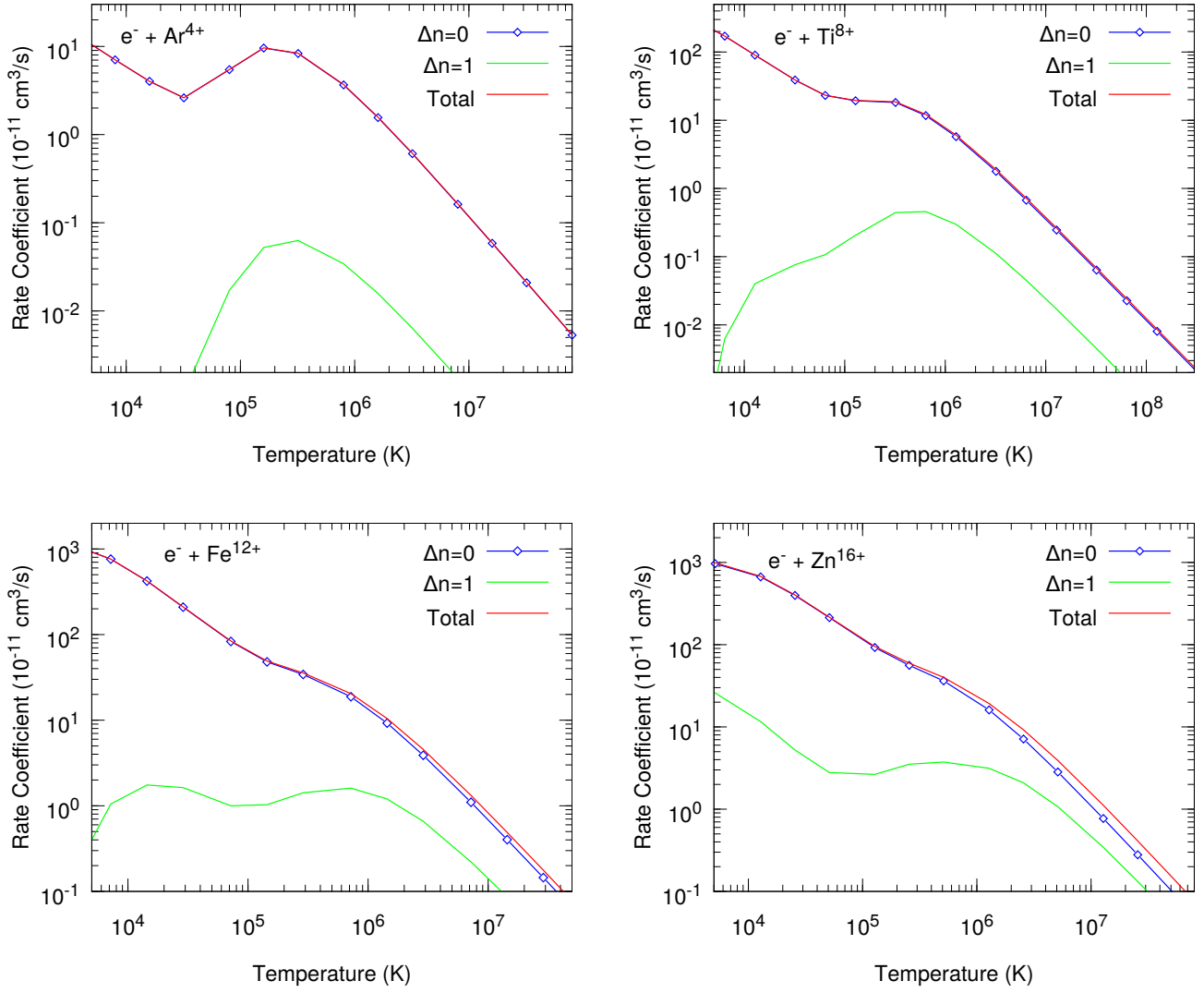


Fig. 6. Total Maxwellian-averaged ground-level DR rate coefficients and the separate contributions from $\Delta n_c = 0$ and $\Delta n_c = 1$ core excitations for Ar^{4+} , Ti^{8+} , Fe^{12+} , and Zn^{16+} ions.

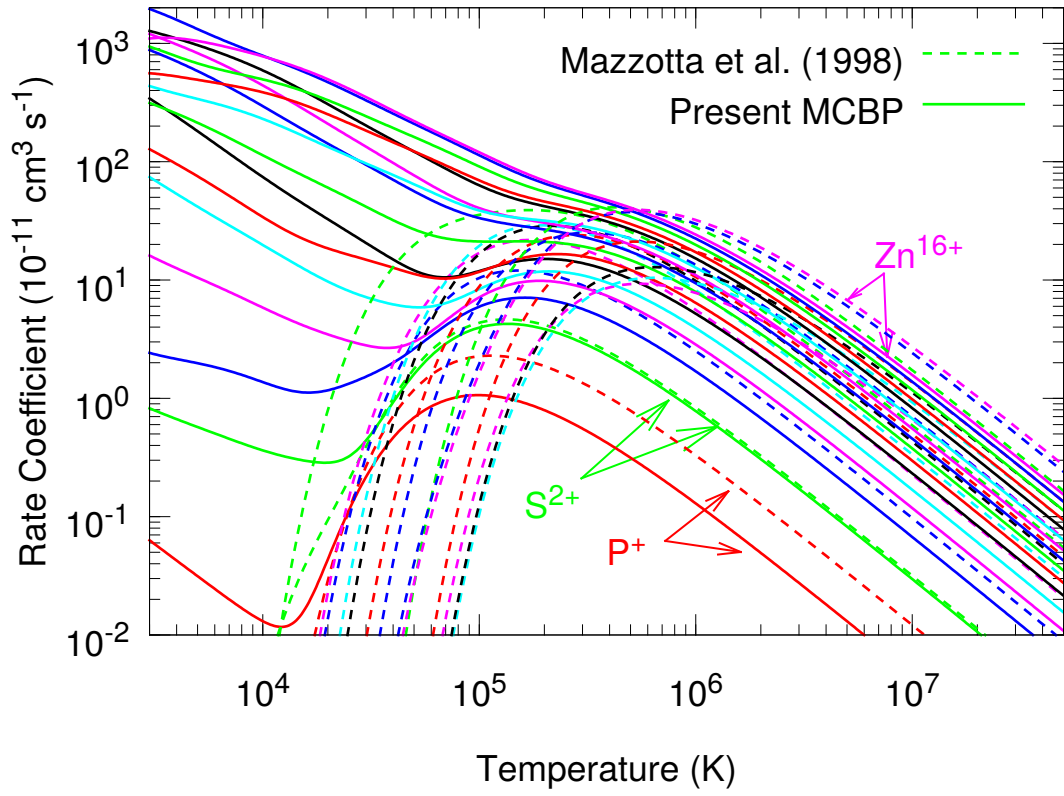


Fig. 7. Comparison between the present total Maxwellian-averaged IC DR rate coefficients (solid curves) and the recommended data (Mazzotta et al. 1998, dashed curves) for the silicon-like isoelectronic sequence.

Table 2. Fitting coefficients c_i (in $\text{cm}^3 \text{K}^{3/2} \text{s}^{-1}$) and E_i (in K) for the total ground-state IC DR rate coefficients.

ion	c_1	c_2	c_3	c_4	c_5	c_6	c_7	c_8
P ⁺	5.128E-08	2.744E-08	2.647E-08	3.652E-08	2.286E-06	9.048E-04	5.975E-04	4.853E-05
S ²⁺	3.040E-07	4.393E-07	1.609E-06	4.980E-06	3.457E-05	8.617E-03	9.284E-04	...
Cl ³⁺	6.019E-07	3.244E-06	2.686E-05	8.945E-04	2.095E-02
Ar ⁴⁺	1.590E-05	1.636E-05	7.566E-05	3.805E-04	5.247E-03	3.272E-02	1.060E-04	...
K ⁵⁺	8.624E-05	8.801E-05	1.934E-04	1.878E-03	4.936E-02	3.667E-03
Ca ⁶⁺	4.836E-04	3.208E-04	9.281E-04	5.307E-02	2.175E-02
Sc ⁷⁺	1.651E-04	2.659E-04	2.517E-03	7.847E-02	1.681E-02
Ti ⁸⁺	4.657E-04	1.194E-03	2.720E-03	3.812E-02	8.260E-02
V ⁹⁺	1.903E-03	2.573E-03	5.861E-03	5.971E-02	8.198E-02
Cr ¹⁰⁺	2.687E-03	4.814E-03	6.995E-03	9.119E-02	8.006E-02
Mn ¹¹⁺	1.040E-03	4.548E-03	1.134E-02	1.253E-01	8.492E-02
Fe ¹²⁺	4.469E-03	8.538E-03	1.741E-02	1.630E-01	8.680E-02
Co ¹³⁺	3.163E-03	1.128E-02	2.548E-02	1.987E-01	9.730E-02
Ni ¹⁴⁺	3.306E-03	1.699E-02	3.525E-02	2.401E-01	1.102E-01
Cu ¹⁵⁺	7.276E-03	2.120E-02	4.385E-02	2.783E-01	1.308E-01	1.513E-03
Zn ¹⁶⁺	9.796E-03	2.209E-02	5.492E-02	3.200E-01	1.495E-01

ion	E_1	E_2	E_3	E_4	E_5	E_6	E_7	E_8
P ⁺	1.684E+01	1.053E+02	4.273E+02	7.150E+03	5.600E+04	1.399E+05	1.676E+05	3.120E+07
S ²⁺	5.016E+01	3.266E+02	3.102E+03	1.210E+04	4.969E+04	2.010E+05	2.575E+05	...
Cl ³⁺	1.077E+02	8.933E+02	9.908E+03	8.465E+04	2.657E+05
Ar ⁴⁺	2.879E+02	1.717E+03	9.917E+03	5.769E+04	2.178E+05	3.191E+05	1.250E+06	...
K ⁵⁺	1.876E+02	2.406E+03	1.482E+04	9.215E+04	3.473E+05	4.806E+05
Ca ⁶⁺	3.497E+02	2.664E+03	3.433E+04	3.149E+05	6.358E+05
Sc ⁷⁺	3.808E+02	4.268E+03	5.687E+04	3.742E+05	8.285E+05
Ti ⁸⁺	8.056E+02	6.038E+03	3.964E+04	2.517E+05	6.006E+05
V ⁹⁺	1.360E+03	7.173E+03	5.168E+04	3.081E+05	7.209E+05
Cr ¹⁰⁺	1.403E+03	8.418E+03	6.683E+04	3.746E+05	8.827E+05
Mn ¹¹⁺	1.521E+03	1.177E+04	7.406E+04	4.268E+05	1.058E+06
Fe ¹²⁺	2.462E+03	1.261E+04	9.330E+04	4.887E+05	1.312E+06
Co ¹³⁺	3.776E+03	1.896E+04	1.067E+05	5.476E+05	1.588E+06
Ni ¹⁴⁺	2.329E+03	1.982E+04	1.156E+05	6.074E+05	1.911E+06
Cu ¹⁵⁺	2.466E+03	2.273E+04	1.338E+05	6.643E+05	2.220E+06	1.217E+07
Zn ¹⁶⁺	5.083E+03	2.462E+04	1.588E+05	7.384E+05	2.615E+06

Table 3. RR fitting coefficients for the ground states of Si-like ions (see Eq. 6).

ion	A ($\text{cm}^3 \text{s}^{-1}$)	B	T_0 (K)	T_1 (K)	C	T_2 (K)
P ⁺	1.505E-09	0.8452	1.707E-02	1.301E+06	0.2467	1.284E+06
S ²⁺	2.478E-11	0.4642	3.294E+02	2.166E+07	0.3351	7.630E+05
Cl ³⁺	1.602E-10	0.6129	5.154E+01	3.056E+07	0.1342	6.808E+05
Ar ⁴⁺	3.939E-10	0.6607	3.207E+01	3.043E+07	0.0761	6.360E+05
K ⁵⁺	6.034E-10	0.6803	3.503E+01	3.022E+07	0.0561	5.412E+05
Ca ⁶⁺	1.427E-08	0.7285	3.790E-01	3.977E+07
Sc ⁷⁺	9.729E-09	0.7294	1.219E+00	3.765E+07
Ti ⁸⁺	7.528E-09	0.7276	3.009E+00	3.764E+07
V ⁹⁺	8.439E-09	0.7289	3.806E+00	3.791E+07
Cr ¹⁰⁺	4.834E-09	0.7238	1.384E+01	3.952E+07
Mn ¹¹⁺	2.598E-09	0.7163	5.391E+01	4.166E+07
Fe ¹²⁺	1.984E-09	0.7101	1.158E+02	4.400E+07
Co ¹³⁺	1.839E-09	0.7055	1.764E+02	4.654E+07
Ni ¹⁴⁺	1.551E-09	0.6991	3.080E+02	4.948E+07
Cu ¹⁵⁺	1.663E-09	0.6970	3.534E+02	5.214E+07
Zn ¹⁶⁺	1.506E-09	0.6920	5.288E+02	5.548E+07